Polariton-polariton interaction constants in microcavities

M. Vladimirova, S. Cronenberger, and D. Scalbert
Groupe d'Etude des Semi-conducteurs, UMR 5650, CNRS–Université Montpellier 2, Place Eugène Bataillon, 34095 Montpellier Cedex, France

K. V. Kavokin
A.F. Ioffe Physico-Technical Institute, 26, Politechnicheskaya, St-Petersburg, Russia

A. Miard, A. Lemaître, and J. Bloch
Laboratoire de Photonique et de Nanostructures, UPR-CNRS, Route de Nozay, 91460, Marcoussis, France

D. Solnyshkov and G. Malpuech
LASMEA, Clermont University-University Blaise Pascal, BP 10448, 63000 Clermont-Ferrand, France and LASMEA, CNRS, UMR 6602, 63177 Aubiere, France

A. V. Kavokin
Dipartimento di Fisica, Universita di Roma II "Tor Vergata," 1, via della Ricerca Scientifica, 00133 Roma, Italy and School of Physics and Astronomy, University of Southampton, Highfield, Southampton SO17 1BJ, United Kingdom

(Received 1 March 2010; revised manuscript received 21 June 2010; published 2 August 2010)

Resonant transmission of light through a microcavity in the strong coupling regime is used to estimate the strength of the interaction between polaritons with parallel (α_1) or antiparallel (α_2) spins. The ratio α_2/α_1 is found to be strongly dependent on the detuning between exciton and photon modes. From negative to zero detuning it changes from about 0 to less than −1. Our observations indicate that at certain conditions the polaritons might rather condense in the real space than form a Bose-Einstein condensate. We analyze theoretically different mechanisms of polariton-polariton interaction including the mean-field electrostatic interaction, the direct exchange interaction, the Van-der-Waals interaction and the indirect exchange interaction via dark exciton and biexciton states.

DOI: 10.1103/PhysRevB.82.075301 PACS number(s): 71.36.+c, 71.35.Lk

I. INTRODUCTION

Exciton-polaritons (polaritons)[1] in planar semiconductor microcavities[2] containing quantum wells are usually formed by heavy-hole excitons and cavity photons.[3] A heavy-hole exciton has four allowed spin projections on the axis of the structure (−2, −1, 1, 2) but only two of them (−1, 1) are coupled to light.[4] Thus, polaritons in microcavities have two allowed spin states, which are degenerate in the absence of external magnetic fields. This is an unusual spin structure for a bosonic quasiparticle: an even number of allowed spin projections is rather characteristic of fermions. Due to their peculiar spin structure, coherent condensates of polaritons exhibit very unusual and interesting polarization properties. These include the self-induced Larmor precession of polarization,[5] the optical spin Hall effect,[6] the "spin Meissner" effect,[7] and formation of half-quantum vortices in polariton superfluids.[8] The polariton-polariton interactions which are crucial for superfluidity and responsible for many other nonlinear effects are strongly spin-dependent. Due to the specific spin structure of polaritons, they can be described using two constants which characterize the strength of interaction of polaritons having identical spin projections to the axis of the cavity (α_1) and the one of those having opposite spin projections (α_2).[9,10]

The parameters α_1 and α_2 have a crucial impact on the critical conditions for the condensation of exciton polaritons in microcavities (see, e.g., Ref. 11). Figure 1 shows the phase diagram of a uniform polariton gas in the coordinates of interaction constants α_1 and α_2. In order to interpret it, let us recall that the free energy of exciton polaritons in an infinite planar cavity at zero temperature can be represented in the form[2,7]

$$F = -\mu n + \frac{\alpha_1 + \alpha_2}{4} n^2 + (\alpha_1 - \alpha_2) S_z^2. \quad (1)$$

Here μ is the chemical potential, n is the concentration of polaritons, S_z is linked with the circular polarization degree of the condensate by $\rho_c = 2S_z/n$. The system must have a minimum free energy at equilibrium. Four regions can be delimited depending on the signs of the quantities α_1, $\alpha_1 + \alpha_2$ and $\alpha_1 - \alpha_2$.

If $\alpha_1 - \alpha_2 > 0$, the minimum of free energy is achieved at $S_z = 0$ so that the polariton gas is linearly polarized (dense hatched regions in Fig. 1). The energy shift of the polariton gas is found by minimization of the free energy over concentration

$$E_{lin} = \mu = \frac{\alpha_1 + \alpha_2}{2} n. \quad (2)$$

Depending on the sign of $\alpha_1 + \alpha_2$, the minimum of the free energy F is achieved either at the minimum or at the maximum of the polariton concentration n. (i) If $\alpha_1 + \alpha_2 > 0$ (region I) the minimum of free energy is achieved at the minimum polariton concentration. The uniform polariton gas is stable and linearly polarized. The uniform distribution of the

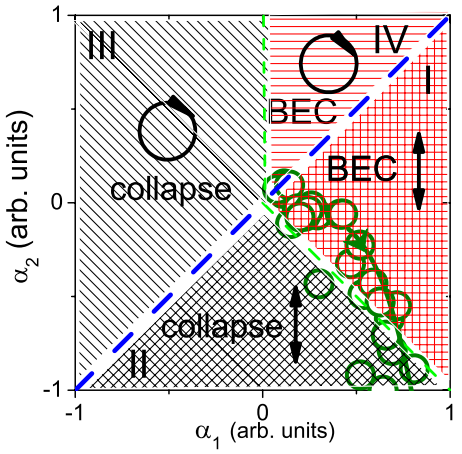

FIG. 1. (Color online) Phase diagram of a gas of interacting exciton-polaritons. Regions of the parameter space corresponding to the real (reciprocal) space condensation are shown by black (red) color. The polarization of the polariton gas is shown by hatching. Dense hatch stands for linearly and rare hatch for circularly polarized state. The values of interaction constants measured at 400 μW excitation intensity for different values of the exciton-photon detuning are shown by circles. Calculated values of the interaction constants are shown by line. The arrow points the direction, where the detuning changes from negative to positive.

condensate in the real space is equivalent to its condensation in the reciprocal space. The Bose-Einstein condensate (BEC) of polaritons is formed in the lowest energy quantum state of the system corresponding to zero in-plane wave vector. (ii) If $\alpha_1+\alpha_2<0$ (region II) the minimum of free energy is achieved at the maximum polariton concentration. There are two possible scenarios of maximization of the polariton concentration. First of all, in a system with a finite number of exciton polaritons, the condensation in real space may take place, in which case the local concentration of polaritons would increase in certain spots of the sample while in the other spots the concentration would decrease. This would lead to the fragmentation of the condensate, similar to what has been observed in Refs. 12 and 13. The location of real-space condensates would be pinned if a lateral potential disorder is present in the cavity. We note that the fragmentation of the condensate is only possible if the increase of its kinetic energy due to localization is weaker than the decrease of polariton-polariton interaction energy. According to Eq. (1), once started, the condensation in real space may go on until the collapse of the condensate. In reality, the increase of polariton concentration would be saturated due to the higher order positive terms in the free energy [omitted in Eq. (1)] which would eventually compensate the decrease of the free energy. If the increase of kinetic energy prevents fragmentation of the condensate and if the condensate is fed by a reservoir of exciton polaritons situated in the excitonlike part of the lower polariton branch, another scenario would be realized. The condensate in this case would accumulate the polaritons while remaining spatially homogeneous. We note that the increase in polariton concentration is actually limited in this regime as well due to the higher order terms in the free energy omitted in Eq. (1).

If $\alpha_1-\alpha_2<0$ the minimum of free energy is achieved at $S_z=\pm n/2$, which means that the polariton gas is circularly polarized (rare hatched regions in Fig. 1). In this case the shift of the polariton energy is

$$E_{circ}=\mu=\alpha_1 n. \tag{3}$$

Depending on the sign of α_1, the minimum of the free energy F is achieved either at the maximum ($\alpha_1<0$, region III) or at the minimum ($\alpha_1>0$, region IV) of the polariton concentration n. In the region IV the polariton gas condenses in the reciprocal space and Bose-Einstein condensation takes place. In the region III classical condensation of exciton polaritons and fragmentation of the condensate in real space are expected for the systems with a finite number of exciton polaritons. If the number of polaritons is unlimited, the virtually unlimited accumulation of polaritons in the condensate would take place, as we discussed above for the region II.

There have been various attempts to estimate α_1 and α_2 from the experimental data[14–17] and to calculate them theoretically.[18–22] The most part of authors believe that these constants should not be strongly dependent on the in-plane wave vector of interacting polaritons if it remains inferior to the inverse exciton Bohr radius. Despite of the deviations between different works, they agree in two essential conclusions: $\alpha_1>0$ and $|\alpha_1|\gg|\alpha_2|$. Some works suggest that α_2 is negative.[14] These conditions are satisfied in the region I of the phase diagram, where a linearly polarized Bose-Einstein condensate is the ground state of the system. The aim of this work is to measure relative values of α_1 and α_2 as a function of the exciton-photon detuning, in order to explore the possibility for polariton condensate to collapse or to acquire circular polarization in the ground state.

In this paper we present the direct measurement of the ratio α_2/α_1 by polarization-resolved nonlinear transmission spectroscopy. The transmission of the square-shaped light pulse tuned to excite the lower polariton branch allows an accurate measurement of its shift due to polariton-polariton interactions. We took advantage of the fact that in the circular basis the energy shift of the polariton states is proportional to α_1 while in the linear basis it is proportional to $(\alpha_1+\alpha_2)/2$. Therefore, the ratio of the polariton shifts measured in linear and circular polarizations is given by $(1+\alpha_2/\alpha_1)/2$ and does not depend on the excitation power (while the interaction constants themselves can depend on the excitation power, in principle). This allows obtaining the ratio α_2/α_1 without any supplementary assumptions.

Our results suggest that at some regions of the sample, in the vicinity of zero detuning between exciton and photon energies, the ratio α_2/α_1 may strongly decrease, so that $\alpha_2/\alpha_1\lesssim-1$. The polariton gas stability analysis as a function of α_1 and α_2 shows that in such region the polariton-polariton interaction in the linearly polarized Bose gas becomes attractive, rather than repulsive. Therefore, a real-space condensation and collapse of Bose-Einstein condensate is expected.[23] Such situation has already been realized in atomic condensates,[24] where a collapse of the Bose-Einstein condensate was induced by application of an external magnetic field.

In the theoretical part of the paper we analyze possible contributions to the polariton pairwise interaction strength, depending on detuning and mutual spin orientation of polaritons. We show that the interaction between polaritons with opposite spins can be attractive ($\alpha_2 < 0$), and at positive detuning it may be as strong as repulsive interaction between polaritons with the same spin. This is mainly due to enhancement of the polariton-polariton exchange interaction via biexciton and dark exciton states with increasing detuning.

The paper is organized as follows. Section II presents the experimental results, and their discussion in terms of the polariton phase diagram. Section III presents possible contributions to polariton-polariton interaction constants while Sec. IV compares experiment and theory. Conclusions are summarized in the last Section.

II. EXPERIMENT

We have studied a GaAs $\lambda/2$ cavity sandwiched between two $AlAs/Al_{0.1}Ga_{0.9}As$ Bragg mirrors (23 and 29 pairs for top and rare mirrors, respectively), grown on the GaAs substrate. An $In_{0.05}Ga_{0.95}As$ quantum well of 8 nm width has been embedded in the middle of the cavity, at the electric field antinode position. The sample has been grown on a wedge (3 meV/mm). In the strong coupling regime, the cavity shows the vacuum field Rabi splitting of 3.5 meV. In order to study the polarization-resolved transmission we illuminated the sample with the square pulses of light of 12 meV spectral width, obtained by spatial filtering of 150 fs pulses of a Ti-sapphire laser. We have been able to excite either both polariton branches simultaneously, or selectively the lower polariton branch. The transmission spectra have been analyzed as a function of the pumping power, polarization and the position of the spot. Because the sample is grown on a wedge, the cavity width changes with the position of the spot on the sample surface. This allows to explore different detuning energies between the exciton and cavity modes. The light beam at normal incidence is focused at a 25-μm-diameter spot on the sample surface. The intensity of light transmitted within the solid angle of 1.5° has been detected using a photomultiplier and spectrally resolved by a monochromator. In order to circumvent the polarization dependence of the monochromator response, light was fully depolarized in the optical fiber of 5 m long. The sample has been placed in the cold finger cryostat at 4 K.

We start our discussion from the results obtained when exciting both polariton branches simultaneously, which is the easiest way to catch the overall behavior of the system. Figure 2(a) shows the map of the linear transmission through the sample at low power and under simultaneous excitation of two polariton branches. On can see that the transmittivity of the sample is substantially reduced in the vicinity of zero detuning. Moreover, the transmittivity appears to be a nonmonotonous function of the detuning. Indeed, the oscillations of the intensity of the transmitted light show up at both branches. We tentatively attribute these oscillations to the substrate corrugations having a characteristic size of 0.4 mm, which induce the absorption variations across the sample. In order to represent the spectra which evidence the polariton

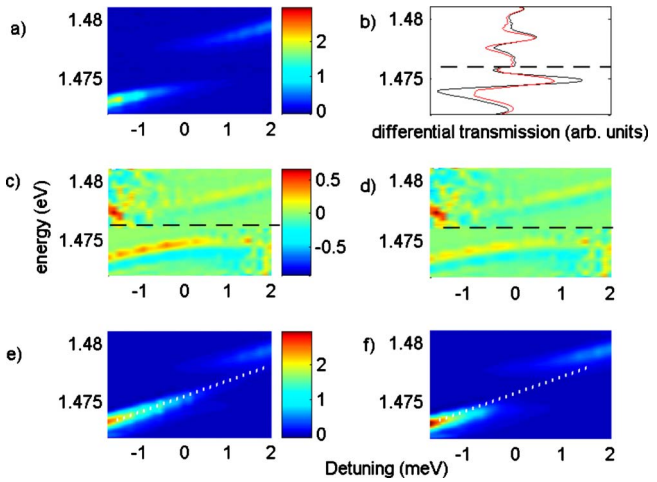

FIG. 2. (Color online) (a) Color map of the low power transmission through the microcavity as a function of detuning between photon and exciton modes; normalized differential transmission spectra in linear (red dashed line) and circular (black solid line) polarizations. (b) The normalization is done independently for lower and upper polaritons (below and above dashed line); color map of the normalized differential transmission $T_{high}-T_{low}$ in (c) circular and (d) linear polarization; color map of the high power transmission at 1.5 mW in (e) circular and (f) linear polarization.

energy shifts as a function of detuning, we use the normalized differential transmission [Fig. 2(b)]. To obtain these spectra we first normalize both low (20 μW) and high (200 μW) power spectra to unity, separately at each polariton branch. Such normalization is mandatory to extract the polariton energy shift from the power-induced modification of transmission, which is directly related to the polariton line shift.[16] After that, the differential transmission ($T_{high}-T_{low}$) at each branch is deduced for each polarization state. The amplitude of differential transmission is proportional to the power-induced shift of the polariton branches. The shape of the signal is that of the first derivative of the transmission peak and its sign is directly related to the sign of the power induced polariton line shift.

Figures 2(c) and 2(d) show the color maps of differential transmission in circular (c) and linear (d) polarizations. The detuning varies along the horizontal axis and the vertical axis shows energy. In both polarizations we observe the oscillations of the differential signal. They are correlated with the oscillations of the transmittivity and will not be important for the physics discussed below. In both polarizations the signal tends to be more important at the low polariton branch but it has the same sign at both branches. As discussed in a previous work,[16] this signifies that both branches exhibit a blue shift, suggesting that the nonlinear effects are mainly due to the exciton resonance shift and not to the variation of the polariton splitting due to reduction in the exciton oscillator strength at high pumping. While at the low polariton branch the difference between circular and linear polarizations is noticeable, it is very tiny at the upper branch. Both the nonlinear shift and the difference between the polarizations disappear when the absolute value of detuning increases.

In principle, the maps of polarization-resolved differential transmission allow the determination of the polariton shift as

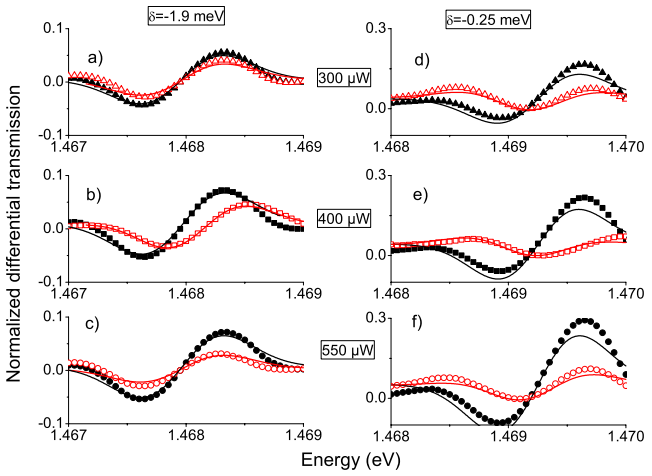

FIG. 3. (Color online) Normalized differential transmission spectra $T_{high}-T_{low}$ of the lower polariton branch at two different photon-exciton detunings: [(a)–(c)] $\delta=-1.9$ meV, [(d)–(f)] $\delta=-0.25$ meV, and at three different pumping power values. Open symbols stand for linear polarization, solid symbols stand for circular polarization. Solid lines are fits with two fitting parameters, namely, the shift and the broadening (narrowing) of the transmission line at high power.

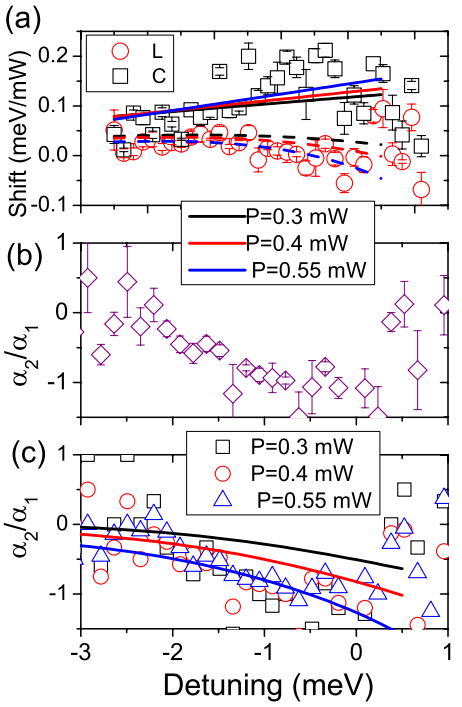

FIG. 4. (Color online) (a) The lower polariton line shift per unit power obtained from the transmission spectra in circular (black squares) and linear (red circles) polarizations. The error bars are given by the averaging over three different excitation powers: 300 μW, 400 μW, and 550 μW. Solid and dashed lines are the values of α_1 and α_2, respectively, calculated as described in the Sec. IV. (b) Ratio between polariton interaction constants averaged over three different powers. (c) The same ratio as in (b) but without averaging. Solid lines show the theoretical results.

a function of pumping power and thus provide the insight to the physics of polariton-polariton interactions. However, a special care should be taken of two factors affecting these maps. First, it is the range of pump powers to study. Indeed, Figs. 2(e) and 2(f) show the transmission maps measured at 1.5 mW, exciting both branches. The Rabi splitting is not reduced at this power and thus the system is still in the strong coupling regime but an additional peak grows up in the transmission spectra, exactly at the energy of the bare photon mode. This third peak appears to be polarization dependent and shows up in circular polarization at the lower pumping power than in linear polarization. It can be understood either in terms of the coexistence of strong and weak coupling,[25] or in terms of purely quantum effects.[26] In this work we limit ourselves to the pumping powers where the polariton shifts are not affected by the third peak, i.e., about 600 μW. The second factor is the excitation of the upper polariton branch. All the spectra shown in Fig. 2 are obtained under simultaneous excitation of two branches. The nonlinear effects measured in this case are affected by interbranch scattering and likely by escape of upper polaritons to the excitonlike part of the lower polariton branch characterized by large in-plane wave vectors.[27] This is why, for the quantitative study of the polariton-polariton interaction we chose the excitation of the lower polariton branch only and we use the excitation powers below 600 μW.

Figure 3 shows a set of normalized differential transmission spectra $(T_{high}-T_{low})$ of the low polariton branch, measured in circular (solid symbols) and linear (open symbols) polarizations for three different powers and two different detunings. The low power (20 μW) means that for such pumping intensity the shifts of the transmission line are close to zero in both circular and linear polarizations. Three different power values were used: 300, 400, and 550 μW. At the most negative detuning (−1.9 meV) the spectra clearly have the shape of the first derivative of the transmission peak, which is a signature of the blue shift of the polariton line. In contrast, at very small negative detuning the shape is more complex, indicative of both shift and broadening of the polariton spectral line with increasing power. In order to extract the polariton shift from the spectra, at each detuning we first fit the low-power transmission with a Gaussian function, and then fit the differential transmission with the difference of two Gaussians. The two fitting parameters are the shift between polariton lines and the broadening. The resulting curves are shown in Fig. 3 by solid lines.

The systematic fits allowed us to extract the polariton energy shift as a function of detuning. The results obtained after averaging over three different pumping powers are shown in Fig. 4(a). One can see that in the vicinity of zero detuning, the polariton energy tends to experience a little redshift in linear polarization, which means that $(\alpha_1+\alpha_2)<0$. This is remarkable, as it signifies that the system may find itself in the Sec. II of the phase diagram (Fig. 1). Indeed, the values of α_1 and α_2 obtained from the measured polariton shifts at 400 μW are shown in Fig. 1 by circles. The arrow points the direction where the detuning increases. One can see that at some points of the sample (close to zero detuning) the system does find itself in the region II of the phase diagram, where the condensation of polaritons in real space is expected.

Figure 4(b) shows the ratio of coupling constants as a function of photon-exciton detuning. For the detunings $\delta < -2$ meV and $\delta > 0$, the distribution of the experimental points is wide, suggesting that the accuracy is poor. This is not surprising because at strong negative detuning the polaritons from the lower dispersion branch have a dominating photon component. Therefore, the polariton-polariton interaction strength is significantly reduced. On the other hand, at positive detuning the transmission itself is very weak because the polariton states at the lower dispersion branch are essentially excitonlike. Thus the polariton energy shifts are difficult to measure. Nevertheless, the overall tendency seems to be the decrease in the α_2/α_1 ratio from nearly zero at negative detuning to about -1 and even less at zero detuning. In order to understand this behavior, we analyze possible contributions to the polariton interaction, taking into account their spin and detuning dependence.

III. ANALYSIS OF POLARITON-POLARITON INTERACTIONS

We calculate the energy shift of the polariton ground state in this system assuming that all polaritons are uniformly distributed in the plane of a quantum well (QW) of width L_z, and can be described by a two-dimensional concentration n. We account for the direct Coulomb and exchange interactions between polaritons as well as for the indirect interactions via the intermediate virtual states.

It is important to note that at the polariton concentrations typical for our experiments (10^{10} cm^{-2}), the average number of polaritons per squared thermal wavelength of the polariton was on the order of 10^2. Therefore, the use of Bose statistics is obligatory. For this reason, we consider interactions within a polariton ensemble described by a many-particle wave function.

A. Blueshift of the exciton-polariton ground state due to direct interactions

1. Mean-field electrostatic energy

This is the energy of electric charges of an electron and a hole forming an exciton in the electrostatic potential formed by other excitons.[28] Obviously, it turns to zero if the electron and hole envelope functions in the normal to the QW plane direction coincide. However, if they are different, the exciton possesses some quadrupole moment so that the mean-field electrostatic energy is different from zero and positive.

If the electron wave function penetrates into the barriers deeper than the hole wave function, the population of excitons in a QW creates an inhomogeneous charge density consisting of a positive sheet at the center of the well and two negative sheets at the edges of the well. The well acts as a plane capacitor in this case. The energy shift induced by this effect per one polariton is given by

$$U_q = 2\pi n X^2 \frac{e^2}{\varepsilon} \int_{-\infty}^{\infty} dz [\xi_h^2(z) - \xi_e^2(z)] \times \int_{-\infty}^{z} dz'(z - z')[\xi_h^2(z') - \xi_e^2(z')], \quad (4)$$

where $\xi_{e(h)}(z)$ is the electron (hole) envelope function in the normal to QW plane direction, ε is the background dielectric constant, e is the electron charge, X is the exciton Hopfield coefficient of the polariton state, which defines the weight of the excitonic contribution to the polariton state. This term is expected to depend nonmonotonously on L_z, having a maximum dependent on the QW geometry and electron and hole masses. The electrostatic interaction is spin-independent and therefore it equally contributes to α_1 and α_2 constants.

2. Direct exchange interaction of polaritons with parallel spins

The exchange interaction of excitons is described by a Hamiltonian[21]

$$H_{ij}^{ex} = -\frac{1}{2} J_{ij}^{ee}(1 + 4\vec{s}_i\vec{s}_j) - \frac{1}{2} J_{ij}^{hh}(1 + 4\vec{j}_i\vec{j}_j), \quad (5)$$

where J_{ij}^{ee} and J_{ij}^{hh} are exchange integrals for electrons and holes, $\vec{s}$ and $\vec{j}$ are electron spin and heavy hole pseudospin, respectively. If the exciton polaritons have parallel spins the exchange contribution to the energy shift is positive and given by the exchange integral.

$$U_{ex}^{d} \approx \pi a_B n X^2 \frac{e^2}{\varepsilon} \quad (6)$$

This term contributes only to α_1.

B. Redshift of the exciton polariton ground state due to indirect interactions

As any second order perturbation process, the indirect interactions reduce the energy of the ground state. Here we consider three types of such interactions: the Van-der-Waals interaction, where the next quantum confined exciton state in a QW serves as an intermediate state;[28] the interaction via optically forbidden exciton states with spins +2 and −2;[29] and interactions via the biexciton state.[22] To calculate the contributions of these interactions to the polariton energy shift, one has to find the matrix element of each of indirect processes between the ground state having N polaritons and the excited state having $N-2$ polaritons. The symmetrized wave function of this excited state can be written as

$$\Psi_{N-2} = \frac{1}{\sqrt{N(N-1)/2}} \sum_{i,j(i<j)} \psi_{ij}. \quad (7)$$

Here ψ_{ij} is the polariton wave function, where ith and jth polaritons are removed to the excited state. The matrix element reads

$$M = \langle \Psi_{N-2} | H_{ind} | \Psi_N \rangle \approx \frac{\sqrt{2}}{N} \sum_{i,j(i<j)} \langle \varphi_i^{ex} \varphi_j^{ex} | H_{ind} | \varphi_i \varphi_j \rangle, \quad (8)$$

where H_{ind} is the Hamiltonian of the indirect interaction, φ_i and φ_i^{ex} are single particle wave functions in the ground (polaritonic) and excited state, respectively. Here we assume $N \gg 1$. If the number of excitations is much less than the total number of polaritons (N), one can introduce the effective Hamiltonian of the system as

$$\tilde{H} = \frac{1}{2}E_1(a^+a + aa^+ - 1) + M(a^+a^+ + aa), \tag{9}$$

where E_1 is the energy difference between the state with a single excitation and the ground state, a^+ and a are creation and annihilation operators of the excitations. By substitution

$$a^+ = \frac{b^+ \cos\vartheta + b \sin\vartheta}{\sqrt{\cos 2\vartheta}}; \quad a = \frac{b \cos\vartheta + b^+ \sin\vartheta}{\sqrt{\cos 2\vartheta}}, \tag{10}$$

where operators b^+ and b satisfy the same commutation relations as a^+ and a, the Hamiltonian is transformed into

$$\tilde{H} = \left(\frac{E_1}{2\cos\vartheta} + M\tan 2\vartheta\right)(b^+b + bb^+) + \left(\frac{E_1}{2}\tan 2\vartheta + \frac{M}{\cos 2\vartheta}\right)(b^+b^+ + bb) - \frac{E_1}{2}. \tag{11}$$

Choosing $\sin 2\vartheta = -2M/E_1$ we obtain

$$\tilde{H} = \frac{E_1}{2}\sqrt{1 - \frac{4M^2}{E_1^2}}(b^+b + bb^+) - \frac{E_1}{2}. \tag{12}$$

The ground state energy of this Hamiltonian is

$$E_0 = \frac{E_1}{2}\left(\sqrt{1 - \frac{4M^2}{E_1^2}} - 1\right) \tag{13}$$

E_0 is negative; if $M \ll E_1/2$, it is approximately equal to $-M^2/E_1$, the result of the second-order perturbation theory.[21] The excitation energy, proportional to the square root in Eq. (13), goes to zero at $2M = E_1$, indicating that the ground state becomes unstable.

1. Van-der-Waals (dipole-dipole) interaction of exciton polaritons

The interaction Hamiltonian in this case is

$$H_{VdW} = \int \vec{P}(\vec{r})\vec{E}(\vec{r})d^3r, \tag{14}$$

where $\vec{P}$ is the dielectric polarization of polaritons and $\vec{E}$ is the electric field produced by this polarization. Since Eq. (13) assumes averaging over all the polaritons, we must substitute $\vec{P}$ and $\vec{E}$ in Eq. (14) with their mean values. In planar structures, the in-plane polarization does not induce any electric field. The exciton polaritons interact with each other due to mixing of their ground states having even electron and hole wave functions with respect to the center of the quantum well with the excited states having either electron or hole wave functions odd with respect to the center of the well. The matrix element of such interaction writes as

$$M_{VdWe,VdWh} = 2\pi n X^2 e^2 \varepsilon^{-1} \int_{-\infty}^{\infty} \xi_{0e,0h}(z)\xi_{1e,1h}(z)\xi_{0e,0h}(z') \times \xi_{1e,1h}(z')(z - z')dzdz', \tag{15}$$

where $\xi_{0e,0h}(z)$ and $\xi_{1e,1h}(z)$ are electron, hole envelope functions in normal to the QW plane direction for the ground and first excited energy levels, respectively. Having in mind that the hole is heaver than the electron, the first excited state would be one having an electron in the ground state and the hole in the first excited state, which is why in the following we shall be interested only in M_{VdWh}. The dipole polarization P_z and electric field E_z induced by exciton polaritons in the normal to the cavity plane direction can be estimated as

$$P_z \approx d_z n X^2/L_z \approx \varepsilon E_z, \tag{16}$$

where d_z is the matrix element of the Z component of dipole moment. Therefore, we obtain for the matrix element

$$M_{VdWh} \approx \sqrt{2}\frac{d_z^2 n X^2}{\varepsilon L_z} \approx e^2 L_z n X^2/\varepsilon. \tag{17}$$

The energy shift of the lowest energy exciton-polariton state due to the Van-der-Waals interaction writes

$$U_{VdW} = \frac{\Delta_{eo}}{2}\left(\sqrt{1 - \frac{(e^2 L_z n X^2)^2}{\varepsilon^2 \Delta_{eo}^2}} - 1\right), \tag{18}$$

where Δ_{eo} is the splitting between the lowest energy exciton-polariton state characterized by even electron and hole wave functions and the next exciton state which has the even electron and odd hole wave functions. The Van-der-Waals interaction is spin-independent and contributes to both α_1 and α_2.

2. Indirect exchange via dark excitons

The average value of the Hamiltonian (5) for two polaritons with opposite spins is zero. Therefore, for linearly polarized polaritons $[\frac{1}{\sqrt{2}}(\uparrow\Downarrow + \downarrow\Uparrow)$ or $\frac{1}{\sqrt{2}}(\uparrow\Downarrow - \downarrow\Uparrow)]$ the energy of direct exchange is one half of that for like-polarized polaritons. The off-diagonal matrix element coupling these states with the states of dark excitons writes

$$\left\langle \frac{1}{\sqrt{2}}(\uparrow\Downarrow \pm \downarrow\Uparrow)_i \frac{1}{\sqrt{2}}(\uparrow\Downarrow \pm \downarrow\Uparrow)_j |H_{ij}^{ex}| \frac{1}{\sqrt{2}}[(\uparrow\Uparrow)_i(\downarrow\Downarrow)_j + (\uparrow\Uparrow)_j(\downarrow\Downarrow)_i] \right\rangle = \pm\frac{1}{2}(J_{ij}^{ee} + J_{ij}^{hh}). \tag{19}$$

Then, we have for the matrix element M_{ex}^{in}

$$M_{ex}^{i} \approx U_{ex}^{d} \tag{20}$$

while the energy difference between the polariton state and the dark exciton state Δ_{bd} stands for E_1 in Eq. (13). For the energy shift induced by the indirect exchange via dark excitons we obtain

$$U_{ex}^{i} = \frac{\Delta_{bd}}{2}\left(\sqrt{1 - \left(\frac{U_{ex}^{d}}{\Delta_{bd}}\right)^2} - 1\right), \tag{21}$$

3. Indirect exchange via a biexciton state

The energy splitting between the relevant biexciton state and the ground exciton polariton state is one half of the sum of excitation energies of the exciton E_{ex} and the biexciton E_{be} minus the energy of the relevant polariton branch E_{pol}

$$\Delta_{be} = \frac{E_{ex} + E_{be}}{2} - E_{pol}. \quad (22)$$

There is no off-diagonal matrix element between the biexciton state and free exciton states, because both are eigenstates of electrons and holes coupled by the Coulomb interaction. However, if we consider exciton polaritons, there is a finite amplitude of absorption of the photon (part of one polariton) by the exciton (part of the other polariton) with formation of a biexciton state. The polaritons should, of course, have opposite spins. The matrix element of this process is on the order of the Rabi frequency times the fraction of the QW volume occupied by excitons. It can be estimated as

$$M_{be} \approx X\sqrt{1-X^2}\hbar\Omega_R \pi a_B^2 n, \quad (23)$$

where Ω_R is the Rabi frequency. For the energy shift induced by the indirect interaction via biexcitons we obtain

$$U_{be} = f\frac{\Delta_{be}}{2}\left(\sqrt{1 - \frac{(1-X^2)(X\hbar\Omega_R \pi a_B^2 n)^2}{\Delta_{be}^2}} - 1\right), \quad (24)$$

where f is a numerical factor on the order of 1. The indirect interaction via biexcitons only contributes to α_2.

IV. COMPARISON WITH THE EXPERIMENT

The constants of polariton-polariton interaction are defined by

$$\alpha_1 n = U_q + U_{VdW} + U_{ex}^d, \quad (25)$$

$$\alpha_2 n = U_q + U_{VdW} + U_{ex}^i + U_{be}. \quad (26)$$

The direct comparison of this theory to the experiment is complicated by the fact that there is an apparent strong deviation between the value of the polariton blueshift due to direct exchange interaction U_{ex}^d given by theory [Ciuti *et al.*[9] and our Eq. (6)] and obtained experimentally. The reasons for this difference are not entirely clear.[16] In order to fit reasonably well our data we need to extract U_{ex}^d from the experiment. We obtain it from the energy shift ΔE_{circ} measured in circular polarization from which the calculated Coulomb and Van-der-Waals interaction energies are subtracted: $U_{ex}^d \approx \Delta E_{circ} - U_q - U_{VdW}$. The resulting polariton line shifts ΔE_{circ} per unit power are shown for three different powers by solid lines in Fig. 4(a). Then, in order to fit the measured ratio α_2/α_1 we also adjust the numerical factor f in the biexciton induced energy shift U_{be} given by the Eq. (24), which was found to be equal to 2. In numerical calculations we have used the following parameters: exciton Bohr radius of a_B=10 nm, the dielectric permittivity $\varepsilon = 13\varepsilon_0$, where ε_0 is the permittivity of the vacuum, exciton binding energy E_b =5 meV, the quantum well width L_z=8 nm, the Rabi splitting $\hbar\Omega_R$=3.5 meV. Bright and dark exciton energy was 1.475 eV, biexciton energy 1.474 eV, energy of the first excited state 1.477 eV. In order to calculate the electron and hole wave functions, we have used the electron and hole effective masses: $m_e = 0.063m_0$, $m_h = 0.5m_0$, where m_0 is the free electron mass, assuming that the effective masses of identical particles are the same in well and barrier materials.

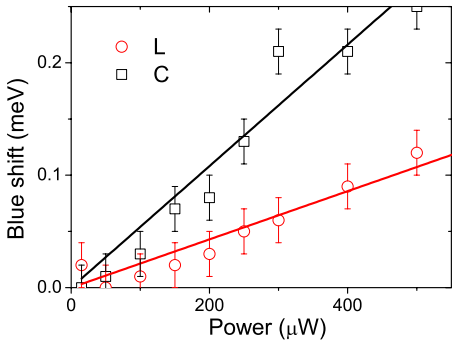

FIG. 5. (Color online) An example of power dependence of the of the lower polariton line shift measured in linear (circles) and circular (squares) polarizations. Solid lines are linear fits of the data.

The barrier heights have been taken V_e=41.4 meV, V_h =32.6 meV for electrons and holes, respectively.

The theoretical results are compared with the experimental data in Fig. 4(b), showing the ratio α_2/α_1 as a function of detuning for three different polariton densities $n = 3.8 \times 10^{10}$ cm^{-2}, $n = 5 \times 10^{10}$ cm^{-2}, and $n = 7 \times 10^{10}$ cm^{-2}. One can see, that α_2/α_1 becomes more negative, as one goes from negative to positive photon-exciton detuning, in agreement with the data. From the theoretical point of view, $|\alpha_2/\alpha_1|$ is also expected to grow with the pumping power but this behavior is not resolved experimentally. Indeed, the power dependence of the polariton line shift in both linear and circular polarizations seems to be linear within the experimental accuracy, as shown in Fig. 5. This justifies averaging of the values of $|\alpha_2/\alpha_1|$ obtained at different pumping powers for each given value of the detuning. To give a reader an idea about the accuracy of the experimentally obtained ratio of the interaction constants we report in Fig. 4(c) the full set of measurements of $|\alpha_2/\alpha_1|$ for three different powers and show the calculation results for comparison. One can see, that the data are strongly dispersed so that the expected power dependence of $|\alpha_2/\alpha_1|$ cannot be resolved. Major amendments of the experimental setup would be required to resolve the nonlinearity of the polariton shifts.

The important experimental result, which is confirmed theoretically, is that the ratio α_2/α_1 may fall below −1 in the vicinity of zero detuning. In this regime, the Bose-Einstein condensation cannot take place and the condensation in the real space would occur instead. This can also be seen in Fig. 1, where the calculated values of the coupling constants α_1 and α_2 for different values of the exciton-photon detuning in the microcavity are shown by a thick solid line.

To compare the relative importance of each mechanism of the polariton-polariton interaction we plot U_q, U_{VdW}, U_{ex}^d, U_{ex}^i, and U_{be} separately as a function of detuning (Fig. 6). One can see that both dipole-dipole and indirect exchange components are negative and remain negligible in the range of the detunings that we explore. The mean-field electrostatic interaction energy is positive, it does not depend on the spin and is supposed to be calculated with relatively good precision using Eq. (4). The direct exchange interaction is determined by the polariton shifts measured in circular polarization, which is why the high values of the ratio α_2/α_1 can only be explained by the strong biexciton term.

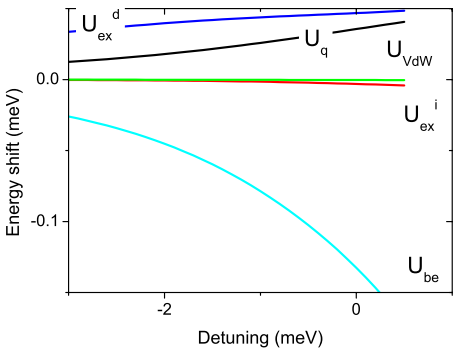

FIG. 6. (Color online) Energies of the lower polariton state (black solid line), bright (red dashed line), and dark (green dotted line) exciton states, excited exciton state (blue dashed-dotted line) as a function of detuning. One can see that both Δ_{oe} and Δ_{bd} splittings decrease when the detuning changes from negative to positive values.

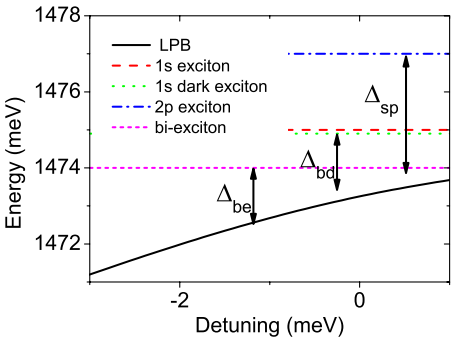

FIG. 7. (Color online) Different contributions to the polariton energy shift due to polariton-polariton interaction.

The detuning dependence of interaction constants can be understood as follows. When the detuning changes from negative to positive, the splittings Δ_{eo}, Δ_{bd}, and Δ_{be} decrease, as illustrated in Fig. 7. Therefore, the contribution of the indirect interactions to the polariton energy shift increases. This influences both α_1 and α_2 constants but α_2 is affected in a greater extent, as neither indirect exchange nor the interaction via biexciton states contribute to α_1.

Finally we note, that despite the apparent agreement between theory and experiment, there is a strong intrinsic deviation between the data and the model. The model explains attraction of polaritons and the negative sign of α_2 by the indirect polariton-polariton interactions via some intermediate states (most likely, biexcitons). The strength of these interactions depends on the polariton concentration, which is why the theory predicts a nonlinear dependence of the polariton energy shift in linear polarization on the pumping power.

Qualitatively, it can be understood in the following way. The probability for each polariton to meet another polariton is proportional to the concentration. Thus the probability of scattering of two polaritons into the virtual intermediate states is also proportional to the concentration. Their scattering back from the virtual states to the condensate is stimulated by the occupation of the condensate, thus its probability is also proportional to the polariton concentration (in the mean-field approximation). Consequently, the product of probabilities of polariton scattering to the virtual states and back to the ground state is proportional to the squared concentration.

Experimentally, we observe no indication of such nonlinear dependence in the power range available in our experiment (Fig. 5). Further studies are needed to achieve better understanding of the mechanisms of polariton attraction in microcavities.

V. CONCLUSIONS

Our measurements show that the amplitude of exciton-polariton interactions is strongly spin-dependent. The excitons with parallel spins attract each other while the excitons with antiparallel spins repel each other. The attraction is weaker than the repulsion at negative photon-exciton detuning that is why the Bose-Einstein condensation of exciton polaritons in planar microcavities is possible. We have found certain regions of our sample, where the attraction is stronger than the repulsion. This indicates the possibility of coexistence of a classical condensate (condensation in real space) and a Bose-Einstein condensate (condensation in reciprocal space) of exciton polaritons within the same sample. The factors responsible for the repulsion of the exciton-polaritons are the mean-field electrostatic interaction (independent on spin) and direct exchange interaction (only for the triplet configuration). The factors responsible for attraction are the Van-der-Waals coupling (independent on spin and small), the indirect exchange coupling via the dark states, and interaction via the biexciton state (main factor). The two latter factors contribute only in the singlet spin configuration. Analyzing the resonant transmission spectra of microcavities in the nonlinear regime, we have obtained a more negative value of the ratio between singlet and triplet polariton-polariton interaction constants α_2/α_1, than that suggested in earlier works.[14–16] The ratio decreases down to about -1, when the detuning changes from negative values to zero. Our model suggests that this is due to the interaction via biexciton states. Measurements at positive detunings are too noisy and do not allow formulating definitive conclusions. However, both theory and experiment indicate that in this regime the ratio of interaction constants can be less than -1, which is crucial for the regime of polariton condensation in microcavities. The Bose-Einstein condensation is expected to be substituted by condensation in real space in this case. Finally, we underline that our results have been obtained on a microcavity sample with a single embedded quantum well. The ratio of interaction constants α_2/α_1 may vary in a different way in the structures containing several quantum wells.

ACKNOWLEDGMENTS

We thank M. Glazov, Y. G. Rubo, and N. Gippius for useful discussions. A.K. and K.K. acknowledge support from the EU IRSES "POLALAS" project. We also acknowledge support from the EU FP7 "CLERMONT4" and "Spin-Optronics" projects.

[1] V. M. Agranovich and O. A. Dubovskii, JETP Lett. **3**, 233 (1966).
[2] A. V. Kavokin, J. J. Baumberg, G. Malpuech, and F. P. Laussy, *Microcavities* (Oxford University Press, Oxford, 2007).
[3] R. Houdré, C. Weisbuch, R. P. Stanley, U. Oesterle, P. Pellandini, and M. Ilegems, Phys. Rev. Lett. **73**, 2043 (1994).
[4] I. A. Shelykh, L. Viña, A. V. Kavokin, N. G. Galkin, G. Malpuech, and R. André, Solid State Commun. **135**, 1 (2005).
[5] I. A. Shelykh, A. V. Kavokin, and G. Malpuech, Phys. Status Solidi B **242**, 2271 (2005).
[6] C. Leyder, M. Romanelli, J. Ph. Karr, E. Giacobino, T. C. H. Liew, M. M. Glazov, A. V. Kavokin, G. Malpuech, and A. Bramati, Nat. Phys. **3**, 628 (2007).
[7] Y. G. Rubo, A. V. Kavokin, and I. A. Shelykh, Phys. Lett. A **358**, 227 (2006).
[8] Y. G. Rubo, Phys. Rev. Lett. **99**, 106401 (2007).
[9] C. Ciuti, V. Savona, C. Piermarocchi, A. Quattropani, and P. Schwendimann, Phys. Rev. B **58**, 7926 (1998).
[10] A. Verger, C. Ciuti, and I. Carusotto, Phys. Rev. B **73**, 193306 (2006).
[11] I. Shelykh, A. V. Kavokin, Y. G. Rubo, T. C. H. Liew, and G. Malpuech, Semicond. Sci. Technol. **25**, 013001 (2010).
[12] M. Richard, J. Kasprzak, R. André, R. Romestain, L. S. Dang, G. Malpuech, and A. Kavokin, Phys. Rev. B **72**, 201301(R) (2005).
[13] J. Kasprzak, M. Richard, S. Kundermann, A. Baas, P. Jeambrun, J. M. J. Keeling, F. M. Marchetti, M. H. Szymanska, R. André, J. L. Staehli, V. Savona, P. B. Littlewood, B. Deveaud, and L. S. Dang, Nature (London) **443**, 409 (2006).
[14] P. Renucci, T. Amand, X. Marie, P. Senellart, J. Bloch, B. Sermage, and K. V. Kavokin, Phys. Rev. B **72**, 075317 (2005).
[15] J. Kasprzak, R. André, L. S. Dang, I. A. Shelykh, A. V. Kavokin, Yuri G. Rubo, K. V. Kavokin, and G. Malpuech, Phys. Rev. B **75**, 045326 (2007).
[16] M. Vladimirova, S. Cronenberger, D. Scalbert, M. Nawrocki, A. V. Kavokin, A. Miard, A. Lemaître, and J. Bloch, Phys. Rev. B **79**, 115325 (2009).
[17] Z. Vörös, D. W. Snoke, L. Pfeiffer, and K. West, Phys. Rev. Lett. **103**, 016403 (2009).
[18] F. Tassone and Y. Yamamoto, Phys. Rev. B **59**, 10830 (1999).
[19] M. Combescot, O. Betbeder-Matibet, and R. Combescot, Phys. Rev. Lett. **99**, 176403 (2007).
[20] S. Schumacher, N. H. Kwong, and R. Binder, Phys. Rev. B **76**, 245324 (2007).
[21] M. M. Glazov, H. Ouerdane, L. Pilozzi, G. Malpuech, A. V. Kavokin, and A. D'Andrea, Phys. Rev. B **80**, 155306 (2009).
[22] M. Wouters, Phys. Rev. B **76**, 045319 (2007).
[23] F. Dalfovo, S. Giorgini, L. P. Pitaevskii, and S. Stringari, Rev. Mod. Phys. **71**, 463 (1999).
[24] E. A. Donley, N. R. Claussen, S. L. Cornish, J. L. Roberts, E. A. Cornell, and C. E. Wieman, Nature (London) **412**, 295 (2001).
[25] P. G. Lagoudakis, M. D. Martin, J. J. Baumberg, G. Malpuech, and A. Kavokin, J. Appl. Phys. **95**, 2487 (2004).
[26] C. Ell, P. Brick, M. Hübner, E. S. Lee, O. Lyngnes, J. P. Prineas, G. Khitrova, H. M. Gibbs, M. Kira, F. Jahnke, S. W. Koch, D. G. Deppe, and D. L. Huffaker, Phys. Rev. Lett. **85**, 5392 (2000).
[27] C. Ciuti, Phys. Rev. B **69**, 245304 (2004).
[28] C. Schindler and R. Zimmermann, Phys. Rev. B **78**, 045313 (2008).
[29] Ł. Kłopotowski, M. D. Martin, A. Amo, L. Vina, I. A. Shelykh, M. M. Glazov, G. Malpuech, A. V. Kavokin, and R. Andre, Solid State Commun. **139**, 511 (2006).